Contrib Mineral Petrol (2011) 161:255–273
DOI 10.1007/s00410-010-0530-2

ORIGINAL PAPER

Chemical composition of spinel from Uralian-Alaskan-type Mafic–Ultramafic complexes and its petrogenetic significance

J. Krause · G. E. Brügmann · E. V. Pushkarev

Received: 24 February 2009 / Accepted: 12 April 2010 / Published online: 26 May 2010

Abstract Uralian-Alaskan-type mafic–ultramafic complexes are recognized as a distinct class of intrusions regarding lithologic assemblage, mineral chemistry and petrogenetic setting. In the present study, we discuss new data on the distribution of major elements in minerals of the spinel group in rocks from Uralian-Alaskan-type complexes in the Ural Mountains, Russia. Cr-rich spinel (Cr_2O_3 = 20–53 wt%) in dunite with interstitial clinopyroxene and in wehrlite cumulates indicate that it reacted with interstitial liquid resulting in the progressive substitution of Al_2O_2 and Cr_2O_3 by Fe_2O_3 and TiO_2. A distinct change in the spinel chemistry in dunite (Cr_2O_3 = 47–53 wt%), towards Al_2O_3- and Cr_2O_3-poor but Fe_2O_3-rich compositions monitors the onset of clinopyroxene fractionation in wehrlite (Cr_2O_3 = 15–35 wt%, Al_2O_3 = 1–8 wt%, Fe_2O_3 = 25–55 wt%). In more fractionated mafic rocks, the calculated initial composition of exsolved spinel traces the sustained crystallization of clinopyroxene by decreasing Cr_2O_3 and increasing FeO, Fe_2O_3 and fO_2. Finally, the initiation of feldspar crystallization buffers the Al_2O_3 content in most of the spinels in mafic rocks at very low Cr_2O_3 contents (<5 wt%). The fractionation path all along and the reaction with interstitial liquid are accompanied by increasing Fe_2O_3 contents in the spinel. This likely is caused by a significant increase in the oxygen fugacity, which suggests closed system fractionation processes. Spinel with $Cr_2O_3 < 27$ wt% is exsolved into a Fe_2O_3-rich and an Al_2O_3-rich phase forming a variety of textures. Remarkably, exsolved spinel in different lithologies from complexes 200 km apart follows one distinct solvus line defining a temperature of ca. 600°C. This indicates that the parental magmas were emplaced and eventually cooled at similar levels in the lithosphere, likely near the crust–mantle boundary. Eventually, these 600°C hot bodies were rapidly transported into colder regions of the upper crust during a regional tectonic event, probably during the major active phase of the Main Uralian Fault.

Keywords Exsolved spinel · Uralian-Alaskan-type complexes · X-ray element mapping · Fractionation · Oxygen fugacity · Chromite

Communicated by C. Ballhaus.

Electronic supplementary material The online version of this article (doi:10.1007/s00410-010-0530-2) contains supplementary material, which is available to authorized users.

J. Krause (✉)
Max-Planck-Institut für Chemie, Becherweg 27,
55020 Mainz, Germany
e-mail: j.krause@mpic.de

J. Krause · G. E. Brügmann
Institut für Geowissenschaften, Universität Mainz,
Becherweg 21, 55099 Mainz, Germany

E. V. Pushkarev
Institute of Geology and Geochemistry,
Russian Academy of Sciences, 620151 Ekaterinburg, Russia

Introduction

Chromian spinel is a vital monitor for the evolution of mafic and, in particular, ultramafic rocks. Its composition gives important information about the degree of partial melting in the mantle or the evolution of mantle melts during rise to the surface (e.g. Irvine 1965; 1967a; Hill and Roeder 1974; Sack and Ghiorso 1991a, b; Van der Veen and Maaskant 1995; Barnes and Roeder 2001). The compositional variation, even on the scale of a single thin section, reports thermodynamic parameters such as temperature and oxygen

fugacity during crystallization processes in lava flows and layered intrusions (e.g. Irvine 1967a; Hill and Roeder 1974; Cameron 1975), as well as late stage magmatic equilibration with interstitial liquid (e.g. Henderson 1975; Henderson and Wood 1981; Roeder and Campbell 1985; Scowen et al. 1991; Candia and Gaspar 1997). The spinel composition is also useful in discriminating between geotectonic settings (e.g. Irvine 1967a; Dick and Bullen 1984; Roeder 1994; Cookenboo et al. 1997; Lee 1999; Barnes and Roeder 2001). However, the spinel composition is subject to considerable subsolidus re-equilibration, such as diffusive mass exchange with neighbouring silicate phases and post-magmatic metasomatic or metamorphic overprint (e.g. Jackson 1969; Springer 1974; Frost 1975; Pinsent and Hirst 1977; Lehmann 1983; Kimball 1990; Melcher et al. 1997; Mellini et al. 2005; Frost and Beard 2007; Iyer et al. 2008). This can result in misleading interpretations concerning tectonic environment and P–T estimates (Power et al. 2000).

Uralian-Alaskan-type mafic to ultramafic complexes define a distinct class of mafic ultramafic intrusions regarding tectonic setting, lithological association and the composition of rock forming and accessory minerals (Taylor and Noble 1960; Noble and Taylor 1960; Irvine 1967b; Findlay 1969; Efimof 1977; Himmelberg et al. 1986; Himmelberg and Loney 1995; Pertsev et al. 2000; Batanova et al. 2005; Krause et al. 2007). Linear belts of Uralian-Alaskan-type complexes, often several hundred kilometres long have been described from the Cordillera of Alaska and British Columbia (e.g. Taylor and Noble 1960; Irvine 1967b; Findlay 1969; Himmelberg et al. 1986; Himmelberg and Loney 1995), on the northern Kamchatka peninsula (e.g. Batanova and Astrakhantsev 1992; Kepezhinskas et al. 1993a,b; Batanova et al. 2005), and in the Ural Mountains, Russia (e.g. Noble and Taylor 1960; Efimof 1977; Ivanov and Shmelev 1996; Pertsev et al. 2000; Chashchukhin et al. 2002; Savelieva et al. 2002; Krause et al. 2007). Characteristic features include the often concentrically zoned association of dunite, wehrlite, clinopyroxenite and mafic rocks, as well as the absence of orthopyroxene in the ultramafic rocks and the setting in elongated belts along convergent margins.

The chemical composition of chromium spinel, in particular its elevated Fe_2O_3-content is another typical feature (e.g. Noble and Taylor 1960; Irvine 1967b; Findlay 1969; Taylor and Noble 1969; Himmelberg et al. 1986; Himmelberg and Loney 1995; Chashchukhin et al. 2002; Krause et al. 2007). This has been ascribed to high total iron contents in the parental melt (Taylor and Noble 1969), fractionation of olivine and clinopyroxene (Findlay 1969; Krause et al. 2007) or an elevated oxygen fugacity (Himmelberg and Loney 1995; Chashchukhin et al. 2002).

Several miscibility gaps occur in the $(Mg,Fe^{2+})_{1+x}(Cr,Al,Fe^{3+})_{2-2x}(Ti)_xO_4$ solid solution series (e.g. Ghiorso and Sack 1991b; Sack and Ghiorso 1991a,b and references therein). At magmatic temperatures, miscibility gaps exist in the $(Fe,Mg)_2TiO_4$–$(Fe,Mg)Al_2O_4$, and at subsolidus conditions in the $MgFe_2O_4$–Mg_2TiO_4, the $FeCr_2O_4$–Fe_3O_4, the $(Fe,Mg)Al_2O_4$–$(Fe,Mg)Cr_2O_4$ and in the $(Fe,Mg)Fe_2O_4$–$(Fe,Mg)Al_2O_4$-series. Exsolution of spinel is described in greenschist to amphibolite facies metamorphic rocks (e.g. Evans and Frost 1975; Loferski and Lipin 1983; Eales et al. 1988; Ozawa 1988; Burkhard 1993; Van der Veen and Maaskant 1995; Candia and Gaspar 1997). However, despite its omnipresence in magmatic rocks, only a few occurrences of exsolved spinel have been described (Muir and Naldrett 1973; Jan et al. 1992; Pushkarev et al. 1999; Garuti et al. 2003; Tamura and Arai 2005; Krause et al. 2007; Ahmed et al. 2008).

The present study focuses on the distribution of major elements in minerals of the spinel group in ultramafic and mafic rocks from Uralian-Alaskan-type complexes in the Ural Mountains, Russia, and discusses the petrogenetic implications. The composition of exsolved and homogeneous spinels indicate the emplacement of the parental magma near the MOHO and monitor the fractionation history of the magma and eventually the post-solidus evolution of the cumulates.

Below, the term ‘spinel’ will be applied for all minerals of the spinel group $(Mg,Mn,Co,Zn,Fe^{2+})_{1+x}(V,Cr,Al,Fe^{3+})_{2-2x}(Ti)_xO_4$. If applicable, we will use more precise terms like ‘chromian spinel’, ‘picotite’, ‘pleonaste’ or ‘chromian magnetite’ as proposed by Deer et al. (1992).

Results

A detailed description of the samples and the analytical methods can be found in the Online Resource 2. The large number of analyses from 35 samples (1,428 of exsolved spinel, 252 of homogeneous chromian spinel and 176 of recalculated exsolved spinel grains) permits only the presentation of selected analyses in Tables 1 and 2 and the Online Resources 4–6. The entire data set is given in the Online Resource 7.

Textural observations among the spinel phases

Homogeneous chromian spinel is present in dunite and wehrlite and in some of the clinopyroxenite samples (NT13, KT39, KT5/290, KT52). These spinel occurs as euhedral to subhedral grains devoid of an optical zonation. Exsolved spinel occurs in dunite from the Tilay-Konjak block (Kytlym), in clinopyroxenite and in nepheline and

Table 1 Composition of selected homogeneous spinels in dunite from the Tilay-Konjak block, Kytlym

Sample	KT310–101	KT310–105	KT310–119	KT310–121	KT310–133	KT311–14	KT311–17	KT311–29	KT311–34	KT311–64	Chromite	Chromite	Chromite
Locality	Til KT	Til KT	Til KT	Til KT	Til KT	Til KT	Til KT	Til KT	Til KT	Til KT	NT	SB	KT
Lithology	Du	Du	Du	Du	Du	Du	Du	Du	Du	Du	Du	Du	Du
Position	R	C	C	C	MR	R	C	C	R	C			
SiO_2	b.d.	b.d.	0.03	0.01	0.12	0.05	0.02	0.02	0.07	0.04	–	–	–
TiO_2	0.67	0.48	0.35	0.44	0.80	1.03	0.47	0.49	1.29	0.73	0.36–0.98	0.33–1.6	0.49–1.52
Al_2O_3	10.14	10.72	9.72	10.53	0.88	3.11	13.69	8.88	5.92	15.86	1.71–10.36	0.08–11.55	5.39–12.06
FeO	45.27	37.86	35.94	38.33	86.83	69.70	36.19	50.58	59.82	35.60	27.15–53.55	28.76–60.74	32.42–52.93
MnO	0.43	0.37	0.37	0.35	0.20	0.31	0.46	0.48	0.36	0.40	0.31–1.28	0.36–1.11	0.32–0.62
MgO	7.73	8.61	8.73	8.93	1.98	2.88	8.27	5.39	4.79	9.29	2.74–11.03	1.33–9.3	3.91–9,4
Cr_2O_3	32.98	40.30	42.97	40.52	1.00	16.74	39.48	30.93	21.66	37.45	34.25–52.39	29.2–52.4	29.45–47.96
NiO	0.17	0.13	0.09	0.11	0.33	0.45	0.16	0.21	0.44	0.16	0.02–0.17	0.07–0.34	0.05–0.21
V_2O_3	0.11	0.05	0.03	0.07	0.07	0.08	0.12	0.05	0.12	0.11	0.01–0.1	0.01–0.2	0.01–0.16
ZnO	0.14	0.17	0.22	0.17	0.02	0.16	0.22	0.34	0.07	0.16	0.06–0.37	0.07–0.27	0.12–0.41
CoO	0.07	0.12	0.09	0.06	0.06	0.08	0.06	0.08	0.09	0.04	0.02–0.22	0.09–0.16	0.04–0.13
Total	97.73	98.86	98.56	99.56	92.29	94.59	99.14	97.49	94.70	99.86	–	–	–
Cr/(Cr + Al)	0.69	0.72	0.75	0.72	0.43	0.78	0.66	0.70	0.71	0.61	0.75–0.93	0.67–0.99	0.63–0.82
$Fe^{3+}/(Cr + Al + Fe^{3+})$	0.34	0.25	0.23	0.26	0.96	0.68	0.21	0.39	0.55	0.21	0.14–0.44	0.14–0.55	0.17–0.42
$Fe^{2+}/(Mg + Fe^{2+})$	0.61	0.57	0.56	0.56	0.89	0.84	0.59	0.72	0.74	0.55	0.45–0.84	0.53–0.92	0.53–0.79
FeO_{calc}	21.44	20.24	19.67	20.02	27.95	27.21	21.20	24.31	24.88	20.57	16.50–27.39	18.71–28.83	19.06–27.77
Fe_2O_{3calc}	26.49	19.58	18.08	20.35	65.43	47.22	16.65	29.19	38.83	16.70	10.72–30.77	10.78–39.69	13.48–31.47

The compositional range of chromite from the other dunite blocks is given for comparison (Krause et al. 2007). *C* core, *R* rim, FeO_m all iron measured as FeO, FeO_{calc} and Fe_2O_{3calc} are calculated assuming stoichiometry, *b.d.* below limit of detection

Table 2 Composition of selected exsolved spinels

Sample	04NT8 c 265	NT8 Spin 266	04NT8 c 244	NT8 Spin 243	NT212 sp 90	NT212 sp 91	04KT50 s 173	04KT50 s 174	04KT50 s 176	04KT50 s 177
Locality	NT	NT	NT	NT	NT	NT	Til KT	Til KT	Til KT	Til KT
Lithology	NeCpx	NeCpx	NeCpx	NeCpx	ByCpx	ByCpx	ByCpx	ByCpx	ByCpx	ByCpx
Composition	M	Pl	M	Pl	M	Pl	M	Pl	M	Pl
SiO_2 (wt%)	0.07	0.05	0.03	0.18	0.08	0.20	0.27	0.28	0.19	0.13
TiO_2	0.64	0.04	1.17	0.05	1.24	0.04	3.68	0.21	2.81	0.11
Al_2O_3	2.92	61.89	1.59	62.99	0.84	63.23	3.39	50.00	2.78	57.17
FeO	83.09	19.50	89.98	19.45	89.69	18.43	74.92	20.96	80.56	18.32
MnO	0.45	0.24	0.29	0.56	0.22	0.30	0.43	0.23	0.33	0.20
MgO	0.59	14.83	0.42	15.57	0.37	16.15	1.53	14.10	0.91	16.31
Cr_2O_3	5.78	1.74	0.85	0.98	0.45	0.50	8.08	11.17	5.46	5.84
NiO	0.10	0.11	0.09	0.13	0.08	0.13	0.27	0.16	0.19	0.18
V_2O_3	0.43	0.03	0.45	0.03	0.45	0.02	0.42	0.07	0.40	0.03
ZnO	b.d.	1.34	0.03	0.54	b.d.	0.31	0.04	1.32	0.03	1.12
CoO	0.02	0.10	0.04	0.10	0.13	0.12	0.12	0.13	0.13	0.12
Total	94.08	99.88	94.95	100.58	93.55	99.42	93.14	98.62	93.78	99.52
Cr/(Cr + Al)	0.570	0.019	0.263	0.010	0.267	0.005	0.615	0.130	0.568	0.064
$Fe^{3+}/(Cr + Al + Fe^{3+})$	0.845	0.022	0.950	0.025	0.973	0.023	0.778	0.053	0.842	0.041
$Fe^{2+}/(Mg + Fe^{2+})$	0.967	0.398	0.977	0.382	0.979	0.362	0.920	0.396	0.952	0.334
FeO_{calc}	30.97	17.51	32.03	17.14	31.61	16.34	31.53	16.45	32.08	14.60
Fe_2O_{3calc}	57.92	2.22	64.40	2.57	64.55	2.32	48.22	5.01	53.88	4.13
Sample	KT35 sp 407	KT35 sp 405	04KT51 271	04KT51 272	KT332-250AB17	KT332-250AB12	KT332-250AB1	KT328 spin 19	KT328 spin 21	KT328 spin 20
Locality	SW-KT	SW-KT	Til KT	Til KT	Til KT	Til KT	Til KT	Til KT	Til KT	Til KT
Lithology	HB i Du	HB i Du	Clin	Clin	Dun	Dun	Dun	Dun	Dun	Dun
Composition	Cm	Pi	Cm	Pi	Cm	U	Pi	Cm	U	Pi
SiO_2 (wt%)	0.09	0.03	0.09	0.05	0.05	0.02	0.03	0.14	0.02	0.02
TiO_2	4.19	0.60	2.21	0.09	1.89	1.87	0.35	2.30	2.41	0.35
Al_2O_3	4.52	32.03	3.82	46.56	7.56	8.60	29.32	4.66	6.35	30.33
FeO	66.77	34.87	76.20	26.11	61.51	59.20	33.65	68.82	63.47	32.67
MnO	0.54	0.38	0.33	0.21	0.48	0.47	0.33	0.42	0.50	0.32
MgO	2.52	9.01	1.27	11.25	3.53	3.83	9.68	2.93	3.27	10.06
Cr_2O_3	18.23	23.03	10.06	14.32	20.89	21.92	25.34	14.41	19.60	25.08
NiO	0.23	0.11	0.11	0.12	0.23	0.26	0.11	0.29	0.20	0.09
V_2O_3	0.34	0.16	0.33	0.03	0.18	0.19	0.09	0.26	0.23	0.09
ZnO	0.09	0.61	0.03	1.36	0.09	0.06	0.31	0.06	0.08	0.37
CoO	0.13	0.13	0.09	0.12	0.07	0.08	0.08	0.04	0.05	0.09

Table 2 continued

Sample	KT35 sp 407	KT35 sp 405	04KT51 271	04KT51 272	KT332-250AB17	KT332-250AB12	KT332-250AB1	KT328 spin 19	KT328 spin 21	KT328 spin 20
Total	97.66	100.96	94.55	100.23	96.48	96.49	99.29	94.32	96.19	99.47
Cr/(Cr + Al)	0.730	0.325	0.638	0.171	0.649	0.631	0.367	0.675	0.674	0.357
$Fe^{3+}/(Cr + Al + Fe^{3+})$	0.597	0.147	0.750	0.063	0.522	0.487	0.158	0.665	0.557	0.149
$Fe^{2+}/(Mg + Fe^{2+})$	0.876	0.592	0.933	0.509	0.818	0.804	0.554	0.846	0.833	0.540
FeO_{calc}	31.81	23.31	31.45	20.77	28.31	27.97	21.44	28.66	28.99	21.05
Fe_2O_{3calc}	38.85	12.85	49.74	5.93	36.90	34.71	13.57	44.63	38.32	12.92

NT Nizhny Tagil, *Til KT* Tilay-Konjak block—Kytlym, *SW-KT* southwest Kytlym, *NeCpx* Ne-clinopyroxenite, *ByCpx* By-clinopyroxenite, *HBDu* hornblendite in dunite, *Clin* Clinopyroxenite, *Dun* dunite, *M* magnetite, *Pi* Picotite, *Cm* chromian magnetite, *Pl* pleonaste, *U* unexsolved core. FeO_m all iron measured as FeO, FeO_{calc} and Fe_2O_{3calc} are calculated assuming stoichiometry, *b.d.* below limit of detection

bytownite clinopyroxenite of all sampled massifs. Three exsolution textures of Fe-rich and Al-rich spinel phases can be observed.

Type A is present in all samples having exsolved spinel regardless of the textural position, the chemical composition and the grain size of spinel. It forms an Al-rich spinel phase (picotite) with an irregular bleb-like texture, predominantly near the rim of spinel grains or along cracks (Online Resource 3d). In some cases, the exsolution might have formed at pre-existing sub grain boundaries. The Fe-rich phase (chromian magnetite) forms the matrix around such blebs. The contacts between both phases are always sharp, have a simple, straight geometry and are well defined by a strong contrast in the reflected light (Online Resource 3d, Krause et al. 2007).

The second texture type B consists of lamellae oriented parallel to the (110) planes which commonly form a network-like texture defined by the appearance of two perpendicular orientations (Fig. 1a). Lamellae have lengths of ten to several hundred micrometres at a typical width of less than 2 μm (Fig. 1a, c). This prevented a precise chemical analysis with the electron microprobe in most of the cases. Type B is limited to spinel with a low Cr content ($Cr_2O_3 < 10$ wt%), and occurs in nepheline and bytownite clinopyroxenite and some clinopyroxenite samples (KT43, KT5-290, KT5-370, KT5-440, KT5-610). Interestingly, the lamellae always consist of an Al-rich spinel in a matrix of Fe-rich spinel. In general, the lamellae are absent in the direct vicinity of type A exsolution (Figs. 1a, c) indicating that the type A exsolution formed prior to the lamellae. In places, a second set of very fine lamellae of Al-rich spinel is present. These lamellae are much smaller and either parallel to the lamellae of the first set or offset with an angle of ca. 30° (Fig. 1c). The two sets of lamellae have no direct contact and are separated by an exsolution-free zone. The lamellae of the second set are interpreted to be younger generation then the larger lamellae of the first set.

The exsolution texture type C has an irregular geometry and predominantly occurs in large spinel grains (>50 μm diameter, Fig. 1d), whereas smaller grains in the same samples mostly show A-type textures. Contacts between the two exsolving phases are commonly diffuse and irregular (detail in Fig. 1d). This texture is restricted to spinels with an intermediate Cr content ($Cr_2O_3 = 15$–35 wt%) that is found in dunite, hornblendite and in one case in a bytownite clinopyroxenite (KT324). Several grains especially in the dunite show also sharp boundaries between both phases with a type A-like texture as an end member. In reflected light, the brighter Fe-rich phase seems to be concentrated at grain boundaries and along healed cracks (CM in Fig. 1d). The cracks are filled with Fe-rich spinel that has an even brighter reflectivity (*M* in

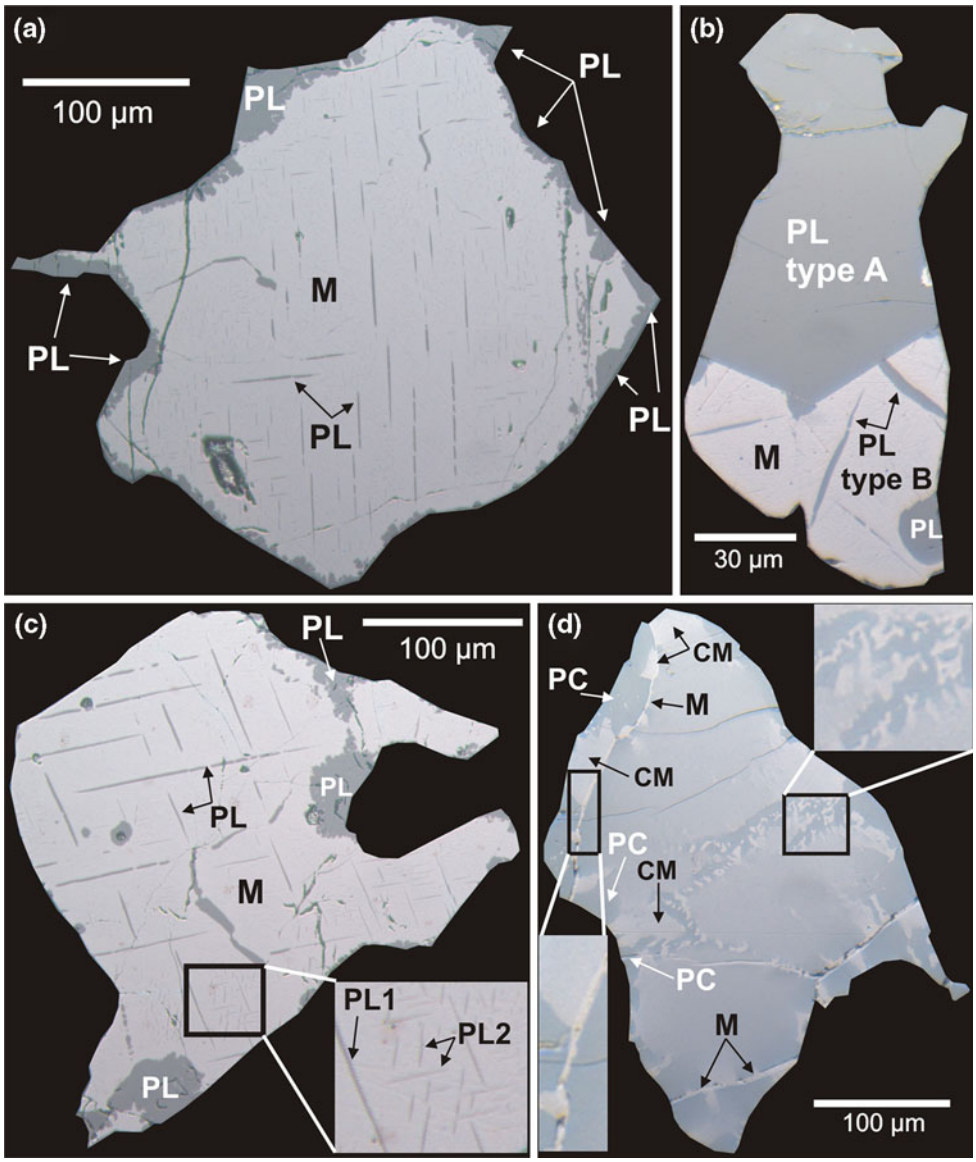

Fig. 1 Reflected light images of exsolution textures in spinel. PL = pleonaste, M = magnetite, PC = picotite, CM = chromian magnetite. **a** Lamellar exsolution type B in the core and blebs of pleonaste in a matrix of magnetite (NT9b). **b** Contact of a lamellar exsolution (type A) and a bleb (type B) of similar composition (NT8). **c** Second generation of fine, lamellar exsolution PL2 forming an angle of 30° with the first generation Pl1 (KT46). **d** Irregular exsolution (type C) concentrated along cracks and grain boundaries (KT328)

Fig. 1d). Remarkably, these spinels often show areas which appear unaffected by any exsolution process.

Spinels in nepheline and bytownite clinopyroxenites and hornblendite frequently are intergrown with ilmenite. It forms one prismatic grain that is often entirely enclosed in spinel.

Textural observations imply that ilmenite exsolved after the formation of bleb and lamellae textures ($A_{(1)}$ and $B_{(2)}$ in Fig. 2) in the spinel, because the straight contact between the ilmenite lamella and the magnetite is interrupted by a picotite-bleb ($A_{(1)}$ in Fig. 2). In addition, the ilmenite encloses an Al_2O_3-rich spinel lamella ($Bi_{(2)}$ in Fig. 2). As ilmenite should not exsolve such spinels, this lamellae must have existed before the formation of ilmenite. This suggests that the TiO_2 content in the primary magmatic spinel is too low to allow the crystallization of ilmenite and that the ilmenite exsolution occurred at temperatures below the solidus. The exsolution process in the primary spinel produced a magnetite which became sufficient Ti-rich to trigger ilmenite exsolution. The Al_2O_3-rich bleb-shaped spinel grains at the rim of ilmenite ($A_{(3)}$ in Fig. 2) probably represent a new generation of Al-rich spinel formed during the ilmenite exsolution. It formed due to the excess of Al_2O_3 available after the breakdown of the Ti-spinel, which cannot be accommodated by the Ti-oxide.

Composition of homogeneous spinels

Homogeneous spinel occurs in dunites from all ultramafic units. Spinels from the Tilay-Konjak block (KT310 and KT311) are slightly more evolved than the spinels in the other dunites covering the low end of the TiO_2, Cr_2O_3,

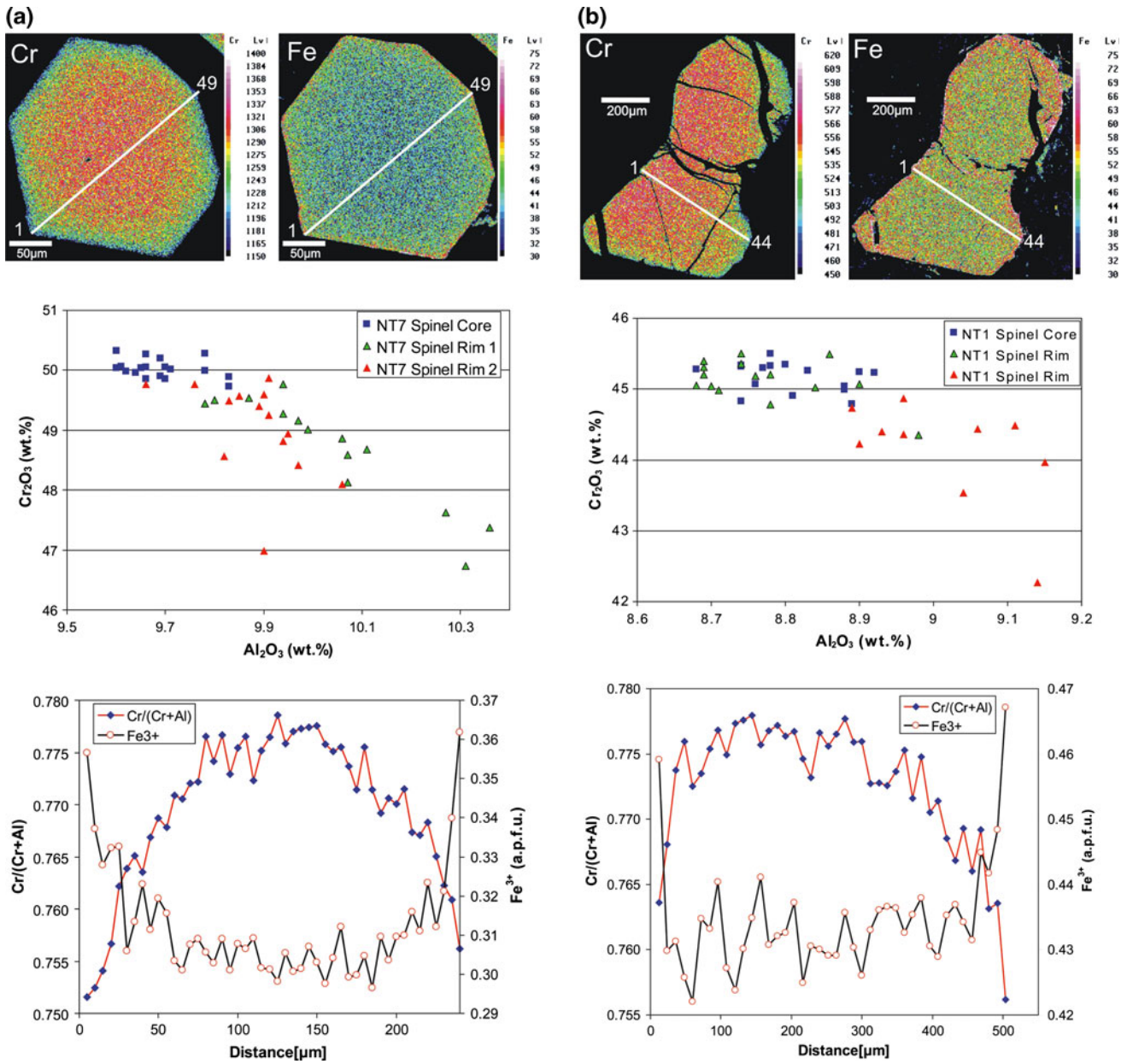

Fig. 2 Compositional variation and spatial distribution of major elements and Cr/(Cr + Al) in homogeneous spinel in dunite. *White lines* in the element distribution maps indicate the position of the profiles of the microprobe analyses. *Rim*1 and *Rim*2 refer to the analyses near both ends of the profile. **a** Symmetric distribution of Cr, Fe_{tot}, Fe^{3+} and Cr/(Cr + Al) in chromite from a dunite containing no interstitial clinopyroxene (NT7). **b** Asymmetric distribution of Cr, Fe_{tot}, Fe^{3+} and Cr/(Cr + Al) in spinel in dunite containing interstitial clinopyroxene (NT1)

Fe_2O_3, $Fe^{2+}/(Mg + Fe^{2+})$, Cr/(Cr + Al) and $Fe^{3+}/(Al + Cr + Fe^{3+})$ variations (Table 1).

X-ray maps and detailed profiles of euhedral chromites in dunite samples from Nizhny Tagil (NT7) and SW-Kytlym (KT40) show a weak but continuous, concentric chemical zoning revealed by an increase in Fe, Mn and Al and a decrease in Cr and Mg contents from core to rim (Fig. 3a). No or inconspicuous zonation is observed for Ti, Ni, V and Co (Online Resource 4). In the Al_2O_3 versus Cr_2O_3 diagram analyses along profiles across the symmetric Cr zonation show a negative correlation as both rims have lower Cr_2O_3 but higher Al_2O_3 contents (Fig. 3a). The Cr/(Cr + Al) decreases while Fe^{3+} increases from the core towards the rim on both sides (Fig. 3a). These variations are expected if the chromite crystallizes from a continuously evolving melt. A post-solidus equilibration with the surrounding olivine can not explain the changes in Al_2O_3 and Cr_2O_3.

In dunite samples with interstitial clinopyroxene, the zonation of Cr in many homogeneous spinels is different in

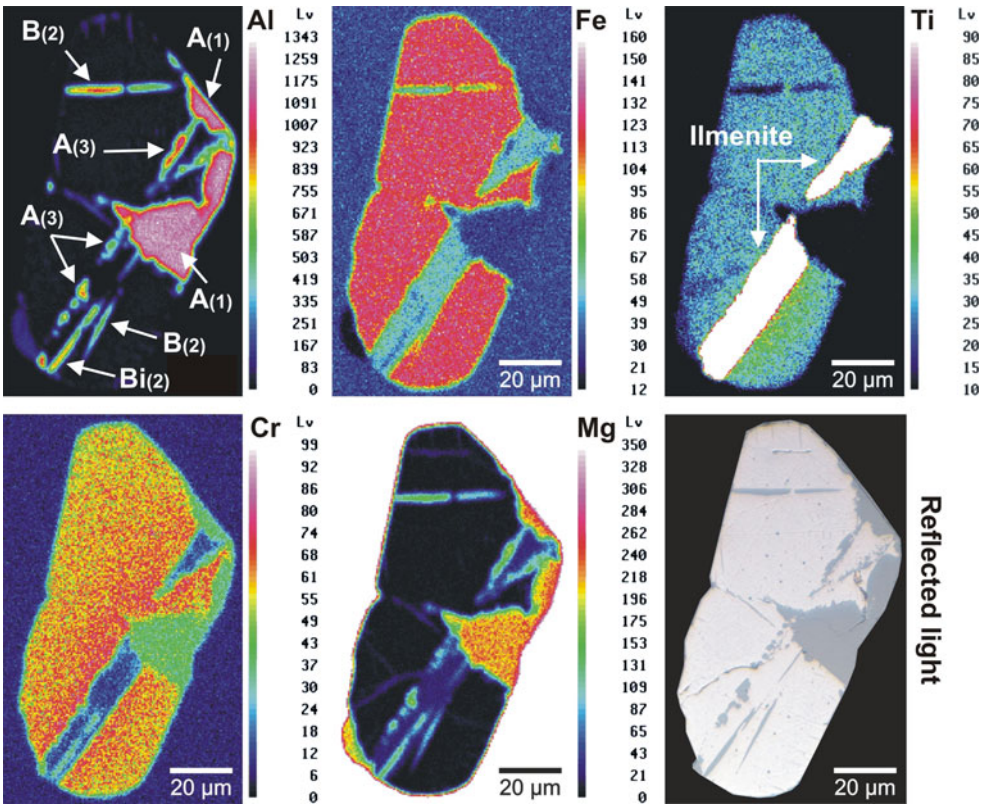

Fig. 3 Element distribution maps for Al, Fe, Ti, Cr and Mg and the reflected light image of exsolved spinel enclosed in olivine from nepheline clinopyroxenite, Nizhny Tagil (NT8). Note the presence of an Al-rich exsolution of the type A at the rim towards the surrounding olivine $A_{(1)}$ and at the boundary of ilmenite with magnetite $A_{(3)}$. Exsolution of the type B are present outside $B_{(2)}$ and inside $Bi_{(2)}$ of a lamella of ilmenite. *Numbers* in brackets denote the order of their formation (for details see text)

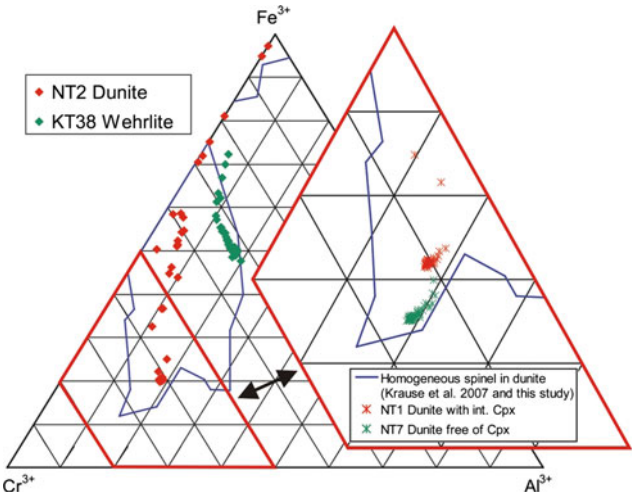

Fig. 4 Distribution of the trivalent cations in the homogeneous spinel shown in Figs. 4 and 6. The spinel in clinopyroxene-bearing lithologies has similar or lower Al_2O_3, but higher Fe_2O_3 contents than that in clinopyroxene-free dunites. Data for compositional variation in homogeneous spinel in dunite from all Uralian complexes are from Krause et al. (2007)

that it is not concentric but crosscuts the concentric zonation patterns of the other elements (Fig. 3b). The zonation pattern has a broad plateau which is defined by high and constant Cr contents. But at the same time, Al_2O_3 systematically decreases. This kind of zonation cannot be attributed to the position of the section plane. However, such grains often occur close to interstitial clinopyroxene suggesting a chemical exchange. There is also a negative correlation of Al_2O_3 and Cr_2O_3 at high Al_2O_3 contents (>8.9 wt%; Fig. 3b), like that observed in the symmetric grains.

In the figure of trivalent cations (Fig. 4), spinel of the clinopyroxene-free dunite with a symmetric distribution of Cr_2O_3 (NT7) forms a trend of decreasing Cr_2O_3 at increasing Al_2O_3 and Fe_2O_3 reflecting the crystallization of the chromite from an olivine crystallizing melt. The trend for chromites from the clinopyroxene-bearing dunite (NT1) with an asymmetric Cr_2O_3 zonation shows an enrichment of Fe_2O_3 at the expense of Cr_2O_3, but no increase in Al_2O_3 (Fig. 4).

Element distributions in some chromite grains from dunite NT2 are distinctly different from those described earlier. In these spinels, Cr/(Cr + Al) and Fe^{3+} variations are positively correlated across the entire grain (Fig. 5a, Online Resource 5). The euhedral grain has a core with an irregular shape which is in composition similar to the previously described chromites. This core is surrounded by a rim of ferrit chromite in composition similar to the outermost rims of the chromites described earlier. The outermost discontinuous rim consists of magnetite (Fig. 5a). Small Ni-sulphide inclusions are present within this zone and at the contact to the core. The contact between the ferrit chromite and the chromite core is sharp and the

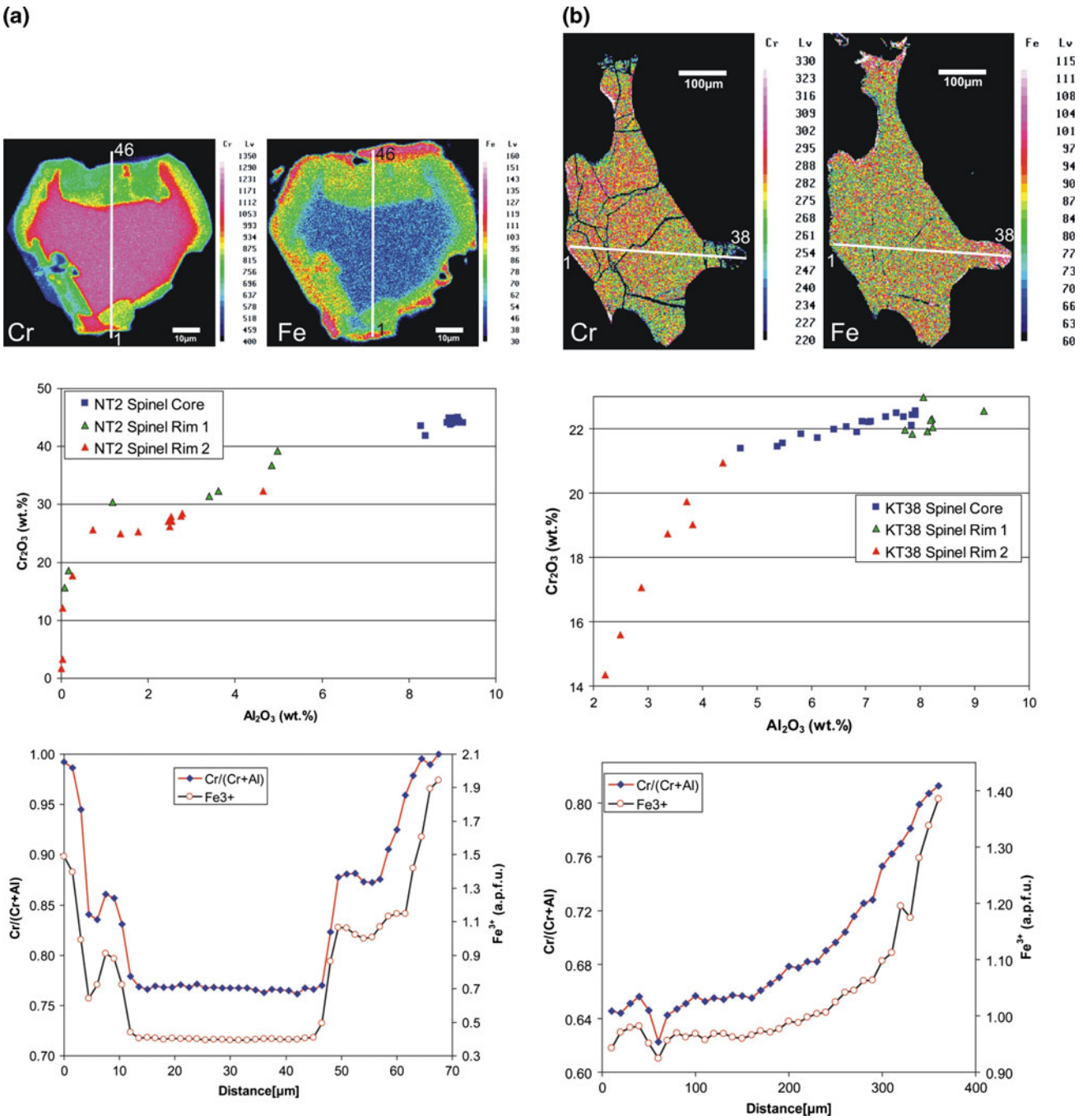

Fig. 5 Compositional variation and spatial distribution of major elements and Cr/(Cr + Al) of homogeneous spinel. **a** Resorbed core of chromite overgrown with chromian magnetite and magnetite (dunite NT2). **b** Anhedral grain with asymmetric distribution of Fe, Cr and Al (wehrlite KT38)

concentration of many elements changes by more than 50% within a distance of less then 5 μm (Fig. 5a). In the Al_2O_3 versus Cr_2O_3 diagram, the core shows a small variation in Al_2O_3 at constant Cr_2O_3. In the ferrit chromite zone, Al_2O_3 decreases more rapidly then Cr_2O_3 (Fig. 5a). The decrease in Cr_2O_3 and Al_2O_3 is balanced by an increase in Fe_2O_3 and MgO is simultaneously replaced by FeO (Online Resource 5). In the trivalent cations diagram, this variation defines the trend of Fe^{3+}-enrichment at the expense of Cr^{3+} and Al^{3+} (Fig. 4).

Spinel in wehrlite from the SW-Kytlym (KT38) has consistently lower Cr_2O_3 and MgO at higher Fe_2O_3 and FeO contents than spinels in dunites (Fig. 5b, Online Resource 5). The grains have an inhomogeneous asymmetric chemical zonation in all major elements with Fe_2O_3 and FeO replacing Al_2O_3, Cr_2O_3 and MgO, respectively

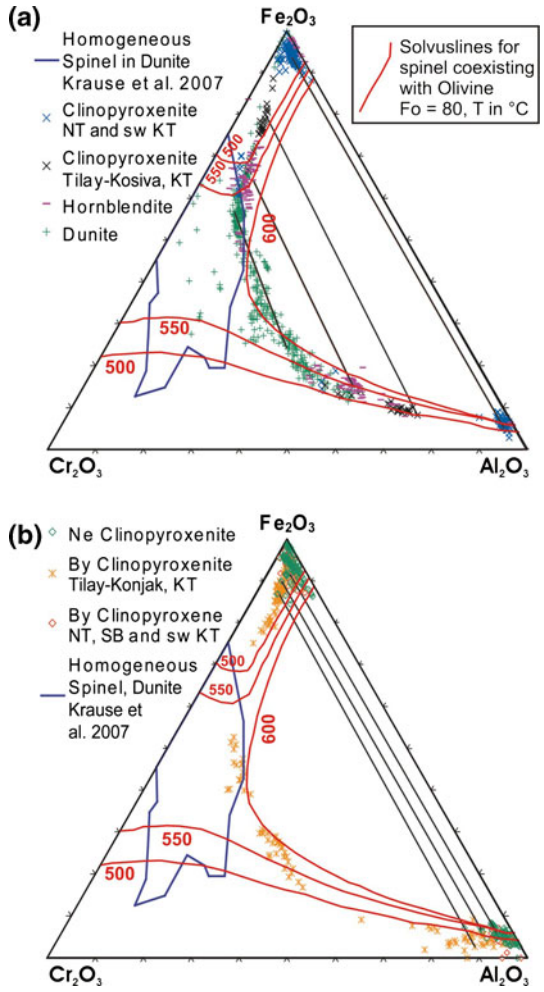

Fig. 6 Variation of the trivalent cations in exsolved spinel from ultramafic rocks (**a**) and mafic rocks (**b**). Solvus curves (*red*) calculated for spinels coexisting with olivine (Fo 80) are taken from Sack and Ghiorso (1991b). Tie lines connect the two exsolved phases in selected grains. The compositions of all spinels lie close along a solvus line suggesting an equilibration at about 600°C. Data for compositional variation in homogeneous spinel in dunite from all Uralian complexes are from Krause et al. (2007)

(Fig. 5b). The Al_2O_3 versus Cr_2O_3 diagram shows at rather constant Cr_2O_3 contents a quick decrease in Al_3O_3; but starting at an Al_3O_3 content of about 4.5 wt%, Cr also decreases strongly (Fig. 5b). This is accompanied by a rapid increase in Fe_2O_3 (Figs. 4, 5b).

Composition of exsolved spinels

The exsolved spinels cover a wide compositional array ranging from pleonaste to picotite and chromian magnetite to almost pure magnetite. Representative analyses can be found in Table 2. In general, the chemical difference of the two exsolved spinel phases increases with decreasing Cr_2O_3-content of the initial spinel. The Fe-rich phase has high contents of TiO_2 (up to 8.1 wt%) and V_2O_3 (up to 1.6 wt%), low contents of MgO (up to 6.9 wt%) and ZnO (up to 0.17 wt%). The coexisting Al-rich phase has higher MgO up to 20.9 wt% and ZnO up to 3.7 wt%. For other components like Cr_2O_3, NiO, MnO and CoO, there is no obvious difference between these two phases (Table 2).

The composition of the exsolved spinel in ultramafic rocks is shifted towards lower Cr/(Al + Cr) relative to the field of homogeneous spinel in dunite. But in terms of $Fe^{2+}/(Mg + Fe^{2+})$ and $Fe^{3+}/(Cr + Al + Fe^{3+})$ the composition of most of the exsolved spinels is similar to that of homogeneous, disseminated spinels from dunites (Online Resource 4; Krause et al. 2007). Type C exsolution with diffuse contacts between both exsolved phases is the dominant exsolution texture in dunite from the eastern part of the Kytlym complex and occurs also in hornblendite. These spinels form a continuous compositional trend ranging from picotite to chromian magnetite. In chromian magnetite with FeO_{tot} <77 wt%, Cr/(Al + Cr) is predominantly controlled by the Al abundance and is systematically higher in the chromian magnetite than in the coexisting pleonaste and picotite. With the exception of a few Cr_2O_3-rich grains in the By-clinopyroxenite from the Tilay-Konjak block all spinels in the mafic rocks and the clinopyroxenites exsolved to magnetite and pleonaste.

In the triangular plot of the trivalent cations, the exsolved spinels plot along a curved line between the Fe_2O_3 and the Al_2O_3 corner (Fig. 6). Spinels with a high Cr_2O_3 content, predominantly from dunite and hornblendite, form a continuous trend that ranges from the Cr_2O_3-poor end of the compositional field defined by the homogeneous spinels towards the Al_2O_3 and Fe_2O_3 corners. Spinel exsolved from Cr_2O_3-poor precursors in the different clinopyroxenites continue this trend almost reaching the pure end member compositions. Remarkably, spinels from all complexes lie along the same line, which represents the solvus curve for spinel coexisting with olivine Fo_{80} at about 600°C (Fig 6; Sack and Ghiorso 1991a,b).

Representative cross-sections of the spinel chemistry across the phase boundaries of coexisting spinels for the three types of exsolution are shown in Fig. 7. The cross-section (A–B) in Fig. 7a is typical for lamellar and bleb-like exsolution textures. The phase boundaries between magnetite and pleonaste are very narrow in both cases (>5 μm) and are defined by a sharp contrast in the concentration of major and minor elements. For example, Fe^{2+}, Fe^{3+}, Ti, V and Mn decrease, while Al, Mg, and Zn increase from the magnetite to the pleonaste (Figs. 7c, e). Chromium, likewise Co, does not change much.

Figure 7b shows a profile (C–D) which is typical for spinels showing the type-C exsolution texture. At about 5 μm close to the rim of the grain, the phase boundary between picotite and chromian magnetite is well defined by its chemical contrast (Fig. 7d, f). Just behind the phase

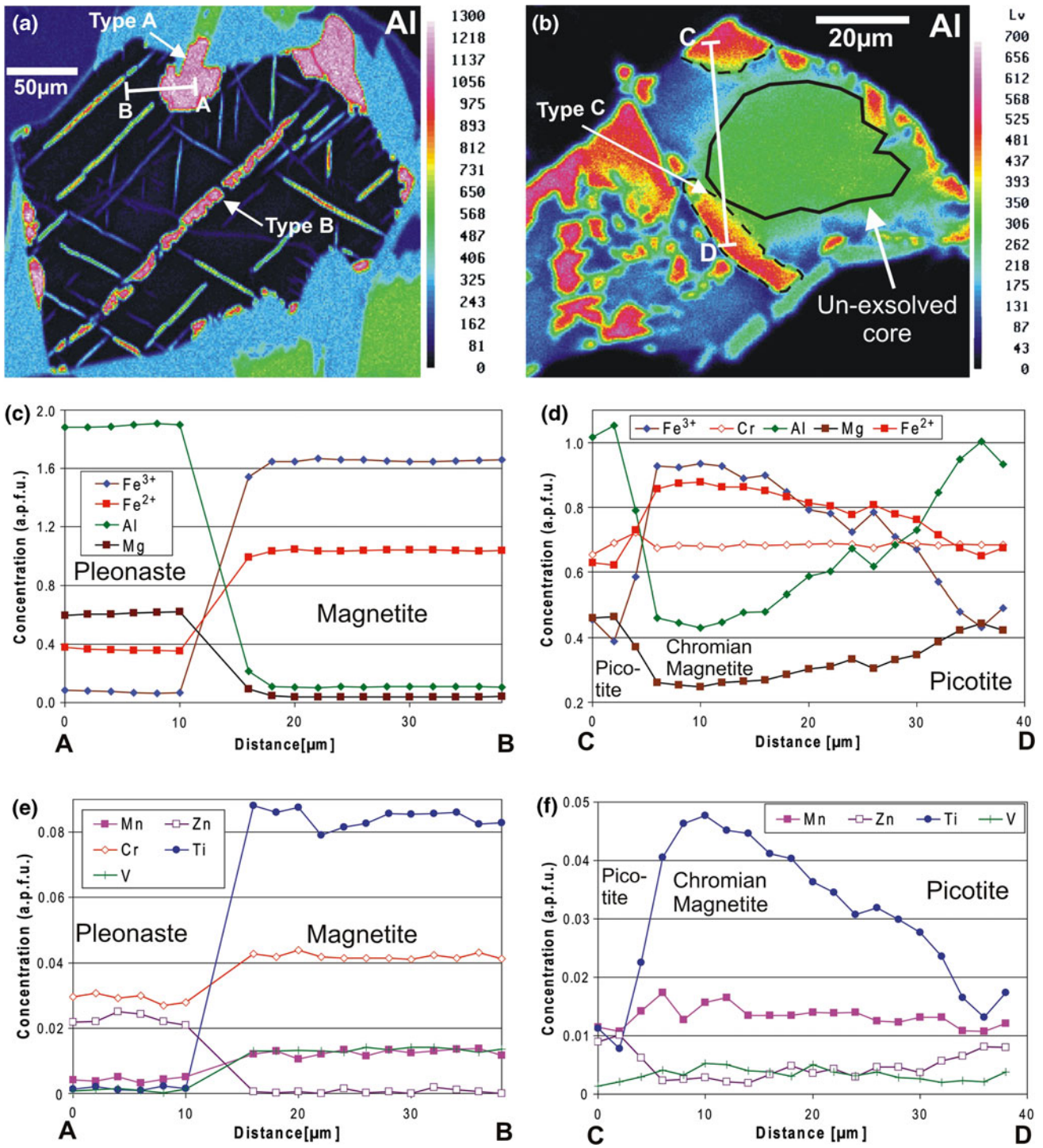

Fig. 7 Variation of minor and major elements across types A and C exsolution textures. **a**, **b** Element distribution maps of Al. **c**, **e** Bleb-like exsolution type A (PE910) with a sharp contrast in the concentration of most elements. **d**, **f** Concentration profiles across exsolution type C with sharp chemical contrast on one and a gradual change in composition at the other side (Dunite from Tilay-Konjak block, Kytlym; KT332). Note the presence of discrete as well as gradual boundaries between the two phases (some are outlined in *dashed black lines*) and the unexsolved core outlined with a *black solid line*

boundary Fe^{3+}, Fe^{2+} and Ti decrease, while Al, Cr, Mg, and Zn increase reaching intermediate compositions (22 and 28 μm in Fig. 7d, f; the green area in Fig. 7a). This phase is interpreted to closely represent the composition of the unexsolved, primary spinel. Along the profile (>28 μm) the spinel eventually approaches a picotite composition

similar to that at the beginning of the profile. The different slopes for the diverse elements may indicate specific diffusivities during the exsolution process.

The recalculated initial composition of exsolved spinels (Table 2) is given in Online Resource 6. Beside its higher Al_2O_3 content, lower Cr/(Cr + Al) and slightly elevated $Fe^{2+}/(Mg + Fe^{2+})$, the calculated composition of spinel in hornblendite and dunite prior to the exsolution is similar to that of homogeneous spinel in dunite (Online Resource 6). These spinels follow chemical trends as described earlier for the homogeneous spinels from the ultramafic rocks. The recalculated primary spinel in the different types of clinopyroxenite from Nizhny Tagil and SW-Kytlym has lower $Fe^{2+}/(Mg + Fe^{2+})$ at a given $Fe^{3+}/(Al + Cr + Fe^{3+})$, if compared to the homogeneous spinel in dunite.

The elevated TiO_2 (>2 wt%) and the lower Cr_2O_3 contents (<6 wt%) in most of the calculated initial spinels from the mafic rocks probably indicate a higher degree of fractionation in the parental melt. Spinel enclosed in olivine and clinopyroxene from By- and Ne-clinopyroxenite has systematically higher Cr_2O_3 and lower $Fe^{2+}/(Mg + Fe^{2+})$, $Fe^{3+}/(Al + Cr + Fe^{3+})$ and Fe_2O_3 than interstitial spinel (Online Resource 6). Recalculated spinel compositions in clinopyroxenite and By-clinopyroxenite from the Tilay-Konjak block (E-Kytlym) indicate higher Cr_2O_3 contents than equivalent rocks from the other localities (Online Resource 6).

Discussion

Evolution of spinel and ilmenite exsolution: implications from petrographic observations and thermodynamic considerations

Lamellar inclusions oriented along well-defined planes of a crystal lattice, such as our type B texture, are classic examples for exsolution textures well known from, e.g. orthopyroxene in clinopyroxene and vice versa, perthite and antiperthite in alkalifeldspar (Putnis 1992), haematite-ilmenite (Haggerty 1991). We suggest that the roundish shape of type-A texture also is the result of an exsolution process. Lamellar and bleb-like textures have similar chemical compositions regardless whether they represent Al-rich or Fe-rich phases, and regardless of the textural position (Fig. 7). Spinel with similar composition and texture have been interpreted as exsolution (e.g. Evans and Frost 1975; Loferski and Lipin 1983; Eales et al. 1988; Haggerty 1991; Tamura and Arai 2005; Ahmed et al. 2008). In all these cases, the coexistence of two spinel phases was attributed to a break-down process either induced by subsolidus cooling/reheating (e.g. Loferski and Lipin 1983; Eales et al. 1988; Ozawa 1988; Jan et al. 1992; Burkhard 1993; Garuti et al. 2003; Tamura and Arai 2005; Ahmed et al. 2008), subsolidus re-equilibration with silicate phases or reactions with coexisting liquid (e.g. Muir and Naldrett 1973; Evans and Frost 1975; Van der Veen and Maaskant 1995; Candia and Gaspar 1997).

Spinodal decomposition and nucleation and growth are proposed as potential mechanisms for the exsolution of ulvöspinel and magnetite from a solid solution (Price 1980; Harrison and Putnis 1997, 1999). Price (1980) assumed a nucleation and growth mechanism along grain boundaries and lattice defects for forming coarse exsolution similar to types A and C. The skeleton of the lamellar type B exsolution could have been initially formed by spinodal decomposition and subsequent coarsening.

Price (1980) and Harrison and Putnis (1997, 1999) also report that, depending on the composition of the spinel prior to the exsolution, an Al-rich host and a Fe-rich guest or a Fe-rich host and an Al-rich guest spinel is formed. This is also observed in the present study, because the Cr_2O_3-content seems to have a dominant control on the geometry of the exsolution textures. Lamellar exsolution (Type B) are restricted to spinels with a Cr_2O_3-content below 10 wt%, thus initial compositions relatively far from the solvus curve at 600°C (Fig. 6). Exsolution textures of type C are found only in spinels with Cr_2O_3 contents above 15 wt% prior to the exsolution. The appearance of texture type A seems not to be controlled by a particular chemical composition of the initial spinel.

Sack and Ghiorso (1991a, b, c) developed thermodynamic models describing the stability of the spinel solid solution in the system $(Mg,Fe^{2+})(Al,Cr,Fe^{3+})_2O_4$ and providing estimates for solvus curves in the trivalent cation plot for a given temperature and forsterite content of coexisting olivine. All exsolved spinels from the Ural mountains, regardless of the lithology and provenance of the sample, plot closely along a single solvus curve indicating a temperature of about 600°C, with a coexisting olivine with compositions of Fo = 80 (Fig. 6). However, olivine with up to Fo95 has been reported from the ultramafic rocks, while Fo contents decrease down to 66 in the By- and Ne-clinopyroxenites (Krause et al. 2007; Krause 2008). Thus, equilibration of spinel with olivine having lower or higher Fo contents may explain the deviations from the calculated solvus in particular those at low Cr_2O_3 fractions. The increase in the $Fe^{2+}/(Mg + Fe^{2+})$ of the recalculated exsolved spinels, from ~0.6 in the ultramafic to ~0.85 in the mafic rocks (Online Resource 6) is accompanied by a decrease in the Fo in coexisting olivine. According to Sack and Ghiorso (1991c) and Ghiorso and Sack (1991a), with decreasing Mg content in spinel the miscibility gap in the system $(Fe,Mg)Fe_2O_4$-$(Fe,Mg)Al_2O_4$ shifts towards more Al-rich compositions. This explains the deviation of the composition of the exsolved Al-rich

phase from the solvus line if one assumes a high Fo = 80 in coexisting olivine.

This cannot explain the misfit between the Fe-rich exsolution products and the calculated solvus curve (Fig. 6). According to Sack and Ghiorso (1991c) and Ghiorso and Sack (1991a) increasing Ti extends the miscibility gap towards the Fe_2O_3 apex. Thus, the high Ti content of the Fe-rich phases in exsolved spinels (Table 2) explains its displacement from the solvus line towards higher Fe_2O_3 proportions. In addition, experimental data by Turnock and Eugster (1962) suggest that the miscibility gap in the trivalent cation plot extends towards the Fe_2O_3 apex with increasing oxygen fugacity. Indeed, the increase in the $Fe^{3+}/(Al + Cr + Fe^{3+})$ in the recalculated exsolved spinels ranging from ~0.4 in dunite to ~0.7 in the clinopyroxenites suggests an increasing oxygen fugacity during fractionation.

Already at temperatures of 550°C, the solvus curve opens up towards Cr_2O_3-rich spinels and reaches the Cr_2O_3-Fe_2O_3-apex in Fig. 6 (Sack and Ghiorso 1991a, b). Thus, spinels in the ultramafic rocks that fall inside the miscibility gap between 550 and 600°C (Fig. 6) should display exsolution textures. In fact, we do not observe exsolved spinels suggesting temperatures of significantly less than 600°C in the Cr_2O_3-rich part of Fig. 6. The presence of homogeneous Cr_2O_3-rich spinel ($Cr_2O_3 > 27$ wt%) in the ultramafic rocks in the direct neighbourhood of exsolved spinel with $Cr_2O_3 < 27$ wt% indicates a common cooling history for these spinels and implies a slow cooling of the host body after its solidification and a final equilibration of spinel at 600°C. Temperatures of about 600°C were estimated in metamorphic mafic–ultramafic rocks containing exsolved spinels with similar composition and textures using independent geothermometers (Ol-spinel) and metamorphic phase equilibria (e.g. Loferski and Lipin 1983; Jan et al. 1992).

Most spinels in clinopyroxenites are Cr_2O_3-poor and lie close to the Al_2O_3-Fe_2O_3-apex in the plot of the trivalent cations (Fig. 6b). According to their Al_2O_3/Fe_2O_3, the exsolution started between 900 and 750°C (Turnock and Eugster 1962; Ghiorso and Sack 1991a). The miscibility gap increases during cooling from this apex towards the centre of the diagram. Therefore, the Cr-poor spinel exsolves first during cooling and the different exsolution textures reflect the complete cooling history of the host body. Spinel with low Cr_2O_3 content has exsolution of type A (blebs) and B (one or two generations lamellae; Fig. 1c). Textural observations (Figs. 1 and 7a, Online Resource 3) indicate that the blebs formed early during the exsolution process, i.e. at the highest temperatures. At this time, the miscibility gap is small and a magnetite with a relatively high Al_2O_3 content and a pleonaste with a significant Fe_2O_3 content are the two exsolving phases. Further cooling enlarges the miscibility gap, forces a continuous re-equilibration of the initial exsolution generation and eventually induces the formation of almost pure magnetite and pleonaste. The excess Al_2O_3 component in magnetite forms crystallographically oriented lamellae of pleonaste. At the same time, FeO, Fe_2O_3 and TiO_2 in the early picotite blebs are redistributed and diffuse into the adjacent magnetite forming pleonaste. This also explains the similar composition of blebs and lamellae within the same grain (Fig. 7). The preservation of two generations of lamellae, separated by a precipitate free zone, presumably reflects the sluggish diffusion at decreasing temperatures preventing complete re-equilibration between the blebs or between the lamellae of the first generation and the surrounding magnetite.

The occurrence of exsolution type C is restricted to Cr_2O_3-rich spinels with an initial composition close to the solvus curve at 600°C. This exsolution started the latest, i.e. at the lowest temperature (Fig. 6b). Some large spinels in the dunites show a transition between type A and C as well as unexsolved areas (Figs. 1d, 7). This indicates that due to the low diffusion rate at the low temperature not all spinel grains could develop the final equilibrium texture of type A. Thus, the exsolution of type C represent an initial stage of type A.

Implications of ilmenite–magnetite exsolutions

Intergrowths of ilmenite lamellae and spinel exsolution occur together in the most fractionated rocks—hornblendites, Ne- and By-clinopyroxenites (Fig. 2). Experimental studies suggest a very low solubility of ilmenite in magnetite at temperatures below 800°C (e.g. Buddington and Lindsley 1964). Accordingly, the observed ilmenite lamellae are interpreted as exsolution of ilmenite and magnetite from a Ti-rich spinel. The absence of ilmenite as a discrete phase in the studied samples supports the interpretation of the ilmenite lamellae being exsolution products.

In our samples, low TiO_2-magnetite coexists with ilmenite with a low magnetite component. Textural observations imply that ilmenite exsolved after the formation of bleb and lamellae textures in the spinel from magnetite which became sufficient Ti-rich to trigger ilmenite exsolution (Fig. 2). In order to exsolve the Ti-rich phase an increase in the oxygen fugacity and/or a decrease in the temperature is required (oxidation exsolution; Buddington and Lindsley 1964; Morse 1980; Eales et al. 1988; Speczik et al. 1988; Lattard et al. 2005; Sauerzapf et al. 2008; Pang et al. 2008). Temperature estimates of coexisting ilmenite and magnetite using the ILMAT geothermometer of Lepage (2003) range from 370 to 615°C and are thus lower than calculations based on the spinel solvus. However, recent experiments performed by Sauerzapf et al. (2008) show that the uncertainty in this

temperature range is large, especially for phases with higher contents in Al_2O_3, MgO, MnO and Cr_2O_3 >6 wt% as it is the case in our samples.

In summary, we recognize the following sequence of oxide formation:

1. Crystallization of homogeneous spinel (spinel 1) together with silicate phases from a mafic–ultramafic melt starting with chromite in the dunites, picotite in the wehrlites and eventually Cr–Ti-bearing magnetite in clinopyroxenite and mafic rocks.
2. Exsolution of an Al- and an Fe-rich spinel from Cr_2O_3-poor spinel 1 in clinopyroxenite when the temperature falls below 900°C. Initial formation of Fe-rich pleonaste blebs in a matrix of Al-rich Ti-magnetite.
3. On further cooling, spinel 1 of some dunites and hornblendites with Cr_2O_3-contents >10 wt% exsolved and formed picotite blebs in a matrix of chromian magnetite. Under the same conditions, the earlier exsolved phases in the spinels from mafic rocks and clinopyroxenite become unstable and Fe and Ti in the pleonaste blebs diffuse into the Ti-magnetite matrix. Excess Al from the magnetite forms one, occasionally two generations of pleonaste lamellae in the magnetite.
4. Exsolution of ilmenite and magnetite from the Ti-magnetite as a reaction to increasing oxygen fugacity and decreasing temperature in hornblendite and mafic rocks. Formation of a second generation of small pleonaste blebs at the interface between ilmenite and magnetite (Fig. 2).

Spinel: a monitor of the evolution of mafic and ultramafic rocks from Uralian-Alaskan-type complexes

Based on the distribution of major and trace elements in clinopyroxene, the characteristic lithological association of dunite, wehrlite, clinopyroxenite and Ne-clinopyroxenite in Nizhny Tagil, Svetley Bor and southwest Kytlym is the result of a complex interplay of igneous processes like the mixing of magmas formed by variable degrees of partial melting in different sources and by fractional crystallization in open magma chamber systems (Krause et al. 2007; Krause 2008). Similarly, the comparison of the chemical compositions of spinel among different lithological units provides detailed information on the crystallization history of the parental magma and the processes during the solidification of the cumulates.

Chemical evolution of spinel in ultramafic cumulates

Variation of oxygen fugacity in parental and derivative melts The low Al_2O_3 content (<10 wt%) in the Cr-rich spinels reflects a rather primitive parental magma composition. This is also indicated by sole crystallization of olivine and spinel, whereas no plagioclase is at the liquidus (Krause et al. 2007). Estimates of the parental melt composition of Uralian-Alaskan-type complexes suggest relatively low Al_2O_3 contents of 8.2–10.7 wt% (Irvine 1973; Pushkarev 2000; Batanova et al. 2005; Thakurta et al. 2008). The most primitive, Cr-richest spinels in dunite samples from all Uralian complexes show a negative correlation in the Al_2O_3 versus Cr_2O_3 (Fig. 8a). This trend is well known from spinels in ocean island basalts, basalt from back arc basins, MORB and boninites (Barnes and Roeder 2001), and it reflects the crystallization of spinel from an evolving ultramafic–mafic melt (Irvine 1967a). The Uralian samples display a considerable Cr_2O_3 variation at Al_2O_3 contents of less than 10 wt% and compared with the basaltic samples have lower Cr_2O_3 and higher Fe_2O_3 at a given Al_2O_3 content (Fig. 8a, b). Besides temperature, pressure and composition of the melt, partitioning of Cr into spinel also depends on the availability of Fe^{3+}, which in turn is controlled by the oxygen fugacity of the melt (Hill and Roeder 1974; Cameron 1975). Thus, the lower and variable Cr_2O_3 content in spinel from the most primitive cumulates in combination with an elevated Fe_2O_3 content at a given Al_2O_3 content suggests that the parental magmas were more oxidized than common upper mantle-derived melts and that there were significant differences in the oxidation states among the parental melts. The redox state in dunite and associated chromitite was determined to vary between 1.9 and 3 logarithmic units above the FMQ buffer by using Moessbauer spectroscopy (Chashchukhin et al. 2002). Estimates of the oxygen fugacity using the model of Ballhaus et al. (1991) tend to be slightly higher (3–4 logarithmic units above FMQ) for the homogeneous spinels in the dunites and systematically increase in the course of fractionation to 4.5–5.5 logarithmic units above FMQ in the mafic rocks (Fig. 8c).

The spinel composition from dunite, wehrlite and clinopyroxenite changes systematically in that Cr_2O_3 and Al_2O_3 contents decrease and Fe_2O_3 and TiO_2 contents increase (Figs. 4 and 9, Online Resource 6). This chemical change is accompanied by decreasing Mg/(Mg + Fe) in coexisting olivine and clinopyroxene (Krause et al. 2007), and hence monitors the fractionation of the parental melt. However, due to the sole crystallization of mafic minerals, one would expect an increase in the Al_2O_3-content in the parental melt, as well as in the crystallizing minerals. Clinopyroxene shows a continuous increase in Al_2O_3 with fractionation, from 0.4 wt% in dunite up to 5.5 wt% in clinopyroxenites (Krause et al. 2007; Krause 2008). Such an increase in Al_2O_3 is not reflected in the spinel composition, in fact the Al_2O_3 content decreases as clinopyroxene starts to crystallize (Figs. 4 and 9; Online Resource 6). This

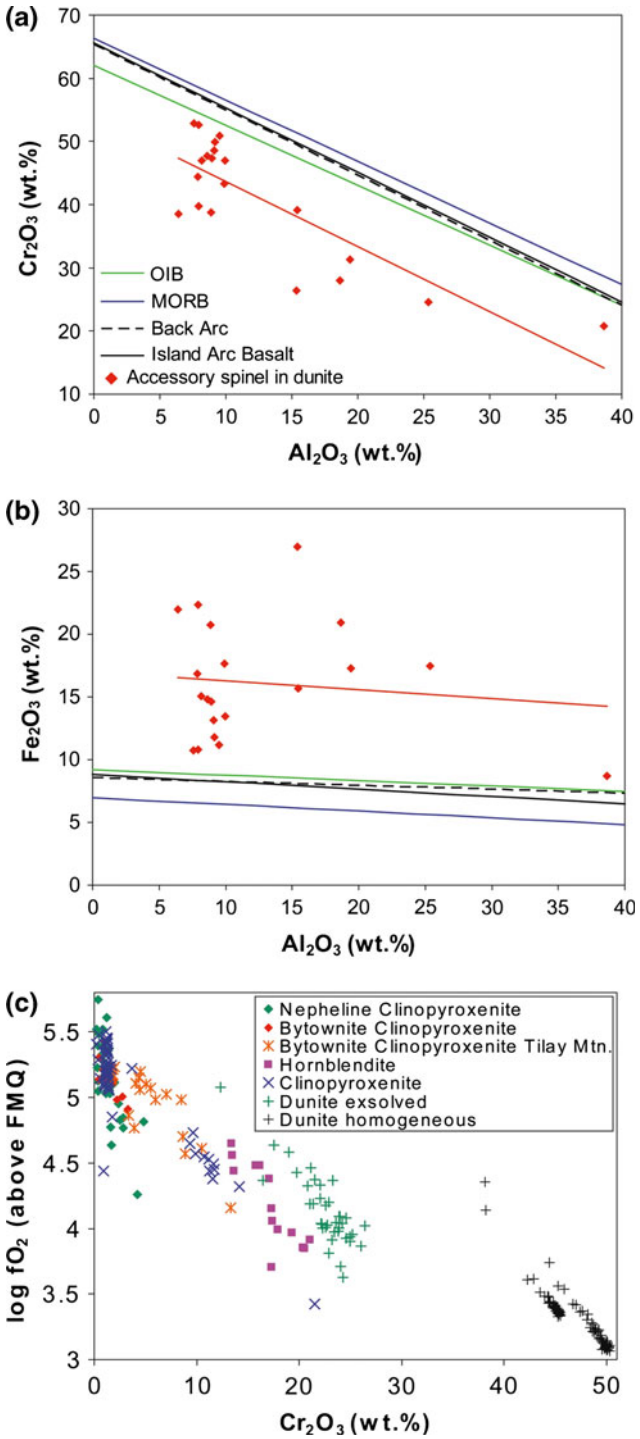

Fig. 8 Variation of Al_2O_3 versus **a** Cr_2O_3 and **b** Fe_2O_3 in homogeneous spinels with the highest Cr_2O_3- content of each dunite sample. The calculated *red trend line* runs parallel to the fractionation trends known from spinel in other tectonic settings (data from Barnes and Roeder 2001). The elevated Fe_2O_3 contents in the studied samples indicate a higher oxygen fugacity in the parental melt. **c** Oxygen fugacity in logarithmic units above the FMQ buffer calculated for the recalculated exsolved spinels using the model of Ballhaus et al. (1991). Compositions for the homogeneous spinels (in *black*) refer to the profiles in Fig. 4. Data for coexisting olivines were taken from Krause (2008)

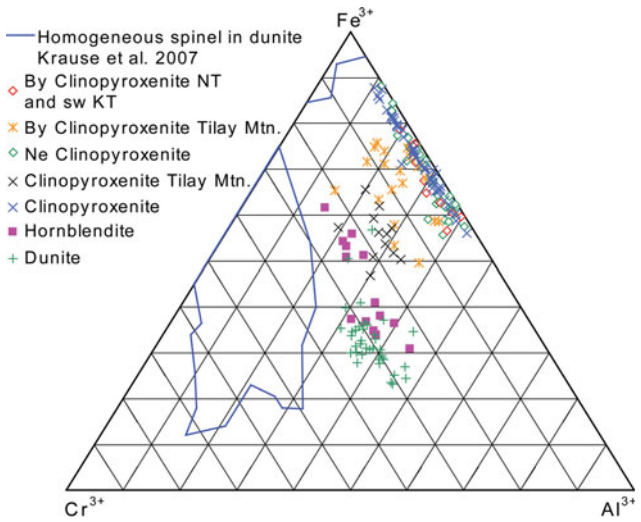

Fig. 9 Variation of the trivalent cations in recalculated exsolved spinel. Cr_2O_3 and Al_2O_3 decrease in the course of fractionation from dunite to clinopyroxenite and nepheline and bytownite clinopyroxenite. Data for compositional variation in homogeneous spinel in dunite from all Uralian complexes are from Krause et al. (2007)

has also been observed in experimental studies (e.g. Irvine 1967a; Hill and Roeder 1974). The low Al_2O_3- but high Fe_2O_3-content in spinel from wehrlite, clinopyroxenite and the mafic rocks should reflect the enhanced competition between Fe^{3+} and Al^{3+} when temperature decreases or the oxygen fugacity of the melt increases during fractionation. An elevated oxidation state is necessary to prevent chromian spinel from getting resorbed and replaced by chromian magnetite when clinopyroxene appears on the liquidus (Hill and Roeder 1974). In the investigated samples, the vast majority of homogeneous spinels do not show resorption features and together with the characteristically high content of ferric iron in the chromite from dunite (Fig. 8), this indicates an initially elevated oxidation state in the parental melt of the ultramafic rocks that further increased in the course of the fractionation. This could be the result of prolonged crystallization of olivine and clinopyroxene which removes preferentially Fe^{2+}, thereby causing an increase in the Fe^{3+} proportion. This process implies a closed system evolution of the magma with regard to the oxygen fugacity.

Interaction of spinel with pore liquid during the solidification of the cumulus pile Some chromian spinels in clinopyroxene-bearing dunite and wehrlite describe a chemical trend that is defined by a non-concentric distribution of Cr and Fe, where Al_2O_3 decreases with decreasing Cr_2O_3 and increasing Fe_2O_3 contents (Figs. 3b, 4, 5a, b). It is a characteristic feature of spinels from Alaskan-type complexes world wide (e.g. Barnes and Roeder 2001; Krause et al. 2007).

Irvine (1967a) and Hill and Roeder (1974) suggested that chromite which initially crystallized together with olivine can be resorbed by a reaction with the melt and clinopyroxene when clinopyroxene starts to crystallize. The irregular shape of the core of a chromite grain from dunite NT2 (Fig. 5a) can be explained by resorption of an early crystallized chromite during its reaction with clinopyroxene-saturated liquid in the pore space. Subsequently, the core has been overgrown with ferrit chromite (Fig. 5a). Crystallization of clinopyroxene from interstitial liquid is supported by its texture and by its extensive enrichment in trace elements, such as REE (Krause et al. 2007). The enrichment of ferric iron is the consequence of the high oxygen fugacity of the interstitial melt and its equilibration with chromite (e.g. Henderson 1975; Henderson and Wood 1981; Roeder and Campbell 1985; Scowen et al. 1991; Candia and Gaspar 1997). The fast equilibration of the Ti^{4+}, Al^{3+} and Fe^{3+} components in spinel with interstitial liquid, even if spinel is enclosed in olivine, has been demonstrated for the Kilauea Iki lava lake on Hawaii (Scowen et al. 1991). Therefore, local re-equilibration of spinel with the interstitial liquid during the cooling of the cumulate pile is a viable process explaining the non-concentric distribution of the trivalent cations in spinel.

Chemical evolution of spinel in mafic cumulates

In the plot of the trivalent cations, the recalculated initial spinel compositions change from Cr-rich towards Fe^{3+}-rich with increasing fractionation (Fig. 9). The initial compositions of spinel in the nepheline and bytownite clinopyroxenites from Nizhny Tagil and SW-Kytlym overlap with those from clinopyroxenites from the same areas (Fig. 9). Taking into account the large uncertainties involved when calculating the initial composition of the exsolved spinels, the Al_2O_3/Fe_2O_3 remains rather constant in the course of fractionation once feldspar is present. This indicates that the Al_2O_3 content of spinel in these rocks is buffered by the cotectic crystallization of feldspar and clinopyroxene.

Disseminated spinel in the Ne- and By-clinopyroxenites from the Tilay-Konjak block has systematically higher $Fe^{2+}/(Mg + Fe^{2+})$, $Fe^{3+}/(Al + Cr + Fe^{3+})$ and Fe_2O_3 and lower Cr_2O_3, if compared to its counterpart enclosed in cumulus clinopyroxene and olivine (Online Resource 6). This can either reflect a fractionation trend, reaction with interstitial melt (Scowen et al. 1991) or a subsolidus re-equilibration with silicate phases (Henderson and Wood 1981). Within the same sample spinel enclosed in clinopyroxene and olivine share the same composition. A systematic mapping of the large clinopyroxene phenocrysts enclosing exsolved spinels did not indicate any significant redistribution of major elements within the clinopyroxene nor between clinopyroxene and spinel. Therefore, the compositional variation in Al_2O_3, Cr_2O_3 and TiO_2 of recalculated spinels enclosed in olivine and clinopyroxene is interpreted to predominantly monitor the fractionation of the parental melt.

Spinel in the different clinopyroxenites from the Tilay-Konjak block (E-Kytlym) has significantly higher Cr_2O_3 contents than spinel from similar lithologies in Nizhny Tagil and southwest Kytlym (Fig. 9). The Tilay-Konjak block lies at the interface of two fundamentally different magmatic plumbing systems and cumulates are interpreted to represent crystallization products from hybrid magmas, which originated from mixing alkaline and tholeiitic parental liquids (Krause 2008). This process could explain the different spinel compositions in the clinopyroxenites from the different areas and probably also reflects the higher Al_2O_3 and lower Cr_2O_3 contents of chromite in the dunites from the Tilay-Konjak block (Table 1), if compared to chromite from dunites in Nizhny Tagil and southwest Kytlym (Krause et al. 2007).

Conclusions

Petrogenetic implications for the evolution of the Uralian-Alaskan-type complexes

The spinel composition traces the petrogenetic processes that form the Uralian-Alaskan-type complexes in the Ural Mountains. The early fractionation of olivine and spinel is monitored by an increase in Al_2O_3 at the expense of Cr_2O_3 in concentrically zoned chromian spinel (Fig. 10). The equilibration of these early chromian spinels with

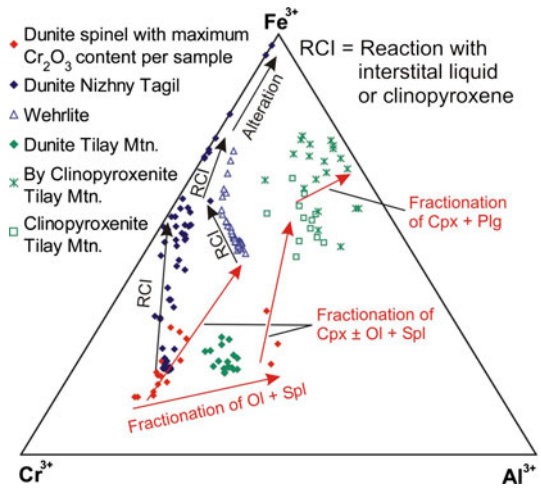

Fig. 10 Trivalent cation plot for selected samples summarizing the evolution of spinel compositions during fractionation processes within and among different lithologies (in *red*) and re-equilibration processes with interstitial liquid or at subsolidus conditions (RCI in *black*). For details, see text

interstitial liquid, which now also crystallizes clinopyroxene, leads in spinel to an increase of Fe_2O_3 and a decrease in first Al_2O_3 and successively Cr_2O_3 (RCI trends in Fig. 10). The chemical variation, in particular, the enrichment of ferric iron in these spinels is similar to trends ascribed to metasomatic (e.g. Mellini et al. 2005; Frost and Beard 2007; Iyer et al. 2008) or metamorphic overprint (e.g. Springer 1974; Frost 1975; Pinsent and Hirst 1977; Kimball 1990). However, any influence of serpentinization or other metasomatic processes on the composition of spinel can be excluded and metamorphic overprint at upper greenschist to amphibolite facies conditions is not known for the Alaskan-type complexes in the Ural Mountains neither supported by our petrographic observations. Thus, a detailed knowledge of the spatial distribution of major elements in spinel and coexisting phases is necessary for applying spinel as indicator for petrogenetic processes or to constrain the geotectonic setting in order to avoid misleading interpretations.

The elevated Fe_2O_3 at low Cr_2O_3 and Al_2O_3 contents in spinel from wehrlite and clinopyroxenite cumulates reflect in part the competing partitioning of Cr_2O_3 and Al_2O_3 from the melt into clinopyroxene and spinel. In addition, the uptake of Al_2O_3 is controlled by the increasing Fe_2O_3 content. This is caused by an increase in the oxygen fugacity suggesting closed system fractionation (Figs. 3, 5, 8c). The onset of the crystallization of feldspar in the nepheline and bytownite clinopyroxenites buffers Al_2O_3 at relatively low levels whereas Cr_2O_3 contents continue to decrease to almost Cr_2O_3-free spinels (Fig. 10).

At temperatures below 900°C and Cr_2O_3 contents below 27 wt%, chromian spinel exsolves two new spinel phases. The exsolution into an Al-rich and a Fe–Ti-rich phase resulted in three different textures indicating nucleation and growth of bleb textures followed by the development of two generations of oriented lamellae in Cr-poor spinels that probably reflect spinodal decomposition. Bleb-like exsolution textures (type A) occur in all exsolved spinels regardless of the chemical composition. Lamellar exsolution (type B) are confined to spinels with Cr_2O_3-contents below 10 wt%, whereas exsolution with diffuse and irregular contacts of both phases (type C) are restricted to spinels with Cr_2O_3 contents above 15 wt%. The Ti-magnetite component of exsolved spinel in hornblendite and nepheline and bytownite clinopyroxenites further exsolved into ilmenite and magnetite. This represents the last equilibration of the oxide phases and indicates further increase in the oxygen fugacity at decreasing temperatures (Fig. 8b). Ilmenite crystallization is accompanied by the formation of a second generation of Al-rich spinel blebs at the phase boundary between ilmenite and magnetite. Almost pure magnetite fills cracks that crosscut the exsolution textures in chromite in dunite and forms in places narrow rims around these grains. Its formation is related to a late serpentinization of olivine (Fig. 10, Online Resource 3d).

In the trivalent cation plot, all exsolved spinels closely match the solvus curve indicating temperatures of 600°C. The similarity of the exsolution temperatures among the different complexes over a distance of several hundred kilometres implies a regional tectonic event that terminated the exsolution process. We consider this temperature to be close to the temperature of the host rocks in which the parental magmas of the Uralian-Alaskan-type complexes formed magma chambers. They gave rise to the different lithologies of dunite, wehrlite, clinopyroxenite and nepheline and bytownite clinopyroxenite cumulates. The depth of the crust–mantle boundary could correspond to the 600°C isotherm above a subduction zone (Tatsumi 1989; Furukawa 1993) and the contrast in density and rheology at this boundary would facilitate the emplacement of mantle-derived melts. This scenario would presume a tectonic environment of a continental or oceanic volcanic arc as proposed for Uralian-Alaskan-type complexes by earlier studies (e.g. Ivanov and Shmelev 1996; Batanova et al. 2005; Krause et al. 2007). Exhumation along regional tectonic structures (e.g. the Main Uralian Fault or the Serov Mauk Fault, Online Resource 1a) transported the complexes into cold upper crustal levels within the Tagil Magnitogorsk-Zone and stopped the re-equilibration process.

Acknowledgments We thank N. Groschopf and B. Schulz-Dobrick for assistance during the microprobe analyses. Chris Ballhaus and two anonymous reviewers are thanked for their helpful suggestions that significantly improved the manuscript. In addition, we would like to thank Chris Ballhaus for his kind editorial handling. This study was funded by grant GK392 of the Graduiertenkolleg 'Stoffbestand und Entwicklung von Kruste und Mantel' at the University of Mainz to J. Krause.

References

Abramoff MD, Magelhaes PJ, Ram SJ (2004) Image processing with imageJ. Biophotonics Int 11(7):36–42

Ahmed AH, Helmy HM, Arai S, Yoshikawa M (2008) Magmatic unmixing in spinel from late Precambrian concentrically-zoned mafic-ultramafic intrusions, Eastern Desert, Egypt. Lithos 104(1–4):85–98

Ballhaus C, Berry RF, Green DH (1991) High pressure experimental calibration of the olivine-orthopyroxene-spinel oxygen geobarometer: implications for the oxidations state of the upper mantle. Contrib Mineral Petrol 107:27–40

Barnes SJ, Roeder PL (2001) The range of spinel compositions in terrestrial mafic and ultramafic rocks. J Petrol 42(12):2279–2302

Batanova VG, Astrakhantsev OV (1992) Tectonic position and origins of the zoned mafic-ultramafic plutons in the Northern Olyutor Zone, Koryak Highlands. Geotectonics 26(2):153–165

Batanova VG, Pertsev AN, Kamenetsky VS, Ariskin AA, Mochalov AG, Sobolev AV (2005) Crustal evolution of island-arc ultramafic magma: Galmoenan pyroxenites-dunite plutonic complex, Koryak Highland (Far East Russia). J Petrol 46:1345–1366

Buddington AF, Lindsley DH (1964) Iron titanium oxide minerals and synthetic equivalents. J Petrol 5:310–357

Burkhard DJM (1993) Accessory chromium spinels: their coexistence and alteration in serpentinites. Geochim Cosmochim Acta 57:1297–1306

Cameron EN (1975) Postcumulus and subsolidus equilibration of chromite and coexisting silicates in the Eastern Bushveld complex. Geochim Cosmochim Acta 39:1021–1033

Candia MAF, Gaspar JC (1997) Chromian spinels in metamorphosed ultramafic rocks from Mangabal I and II complexes, Gioás, Brazil. Mineral Petrol 60:27–40

Chashchukhin IS, Votyakov SL, Pushkarev EV, Anikina E (2002) Oxithermobarometry of ultramafic rocks from the Ural Platinum Belt. Geochem Int 40(8):762–778

Cookenboo HO, Bustin RM, Wilks KR (1997) Detrital chromian spinel compositions used to reconstruct the tectonic setting or provenance: Implications for orogeny in the Canadian Cordillera. J Sediment Res 67(1):116–123

Deer WA, Howie RA, Zussman J (1992) An introduction to the rock-forming minerals, 2nd edn. Pearson, Harlow, pp 558–568

Dick HJB, Bullen T (1984) Chromian spinel as a petrogenetic indicator in abyssal and alpine-type peridotites and spatially associated lavas. Contrib Mineral Petrol 86:54–76

Duparc L, Tikhonowitch M (1920) Le platine et les gites platiniferes de l'Oural et du Monde, Geneve

Eales HV, Wilson AH, Reynolds IM (1988) Complex unmixed spinels in layered intrusions within an obducted ophiolite in the Natal-Namaqua mobile belt. Miner Depos 23:150–157

Efimof AA (1977) Hot tectonics in the hyperbasics and gabbroides of the Urals. Geotektonika 1:24–42 (in Russian)

Efimof AA, Efimova LP (1967) The Kytlym platiniferous massif. Leningrad Nedra 1–356 (in Russian)

Evans BW, Frost BR (1975) Chrome-spinel in progressive metamorphism—a preliminary analysis. Geochim Cosmochim Acta 39:959–972

Findlay DC (1969) Origin of the Tulameen ultramafic-gabbro complex, southern British Columbia. Can J Earth Sci 6:399–425

Frost RB (1975) Contact metamorphism of serpentinite, chloritic and blackwall and rodingite at Paddy-Go-Easy Pass, Central Cascades, Washington. J Petrol 16(2):272–313

Frost RB, Beard JS (2007) On silica activity and serpentinization. J Petrol 48(7):1351–1368

Furukawa Y (1993) Magmatic processes under arcs and formation of the volcanic front. J Geophys Res 98(B5):8309–8319

Garuti G, Pushkarev EV, Zaccarini F, Cabella R, Anikina E (2003) Chromite composition and platinum-group mineral assemblage in the Uktus Uralian-Alaskan-type complex (Central Urals, Russia). Miner Depos 38:312–326

Ghiorso MS, Sack RO (1991a) Thermochemistry of the oxide minerals. Lindsley DH (ed) Oxide minerals petrogenetic and magnetic significance. Reviews in Mineralogy 25 Mineralogical Society of America, Chelsea: pp 221–302

Ghiorso MS, Sack RO (1991b) Fe-Ti oxide geothermometry: Thermodynamic formulation and the estimation of intensive variables in silicic magmas. Contrib Mineral Petrol 108:485–510

Gillespie MR, Styles MT (1999) BGS rock classification scheme volume I classification of igneous rocks. Brit Geol Surv Res Rep 2nd edn. RR 99-06: 1–52

Haggerty SE (1991) Oxide textures—A mini-atlas. In: Lindsley DH (ed) Oxide minerals petrogenetic and magnetic significance. Reviews in Mineralogy 25 Mineralogical Society of America, Chelsea: 129–220

Harrison RJ, Putnis A (1997) Interaction between exsolution microstructures and magnetic properties of the magnetite–spinel solid solution. Am Mineral 82:131–142

Harrison RJ, Putnis A (1999) The magnetic properties and crystal chemistry of oxide spinel solid solutions. Surv Geophys 19:461–520

Henderson P (1975) Reaction trends shown by chrome-spinels of the Rhum layered intrusion. Geochim Cosmochim Acta 39:1035–1044

Henderson P, Wood RJ (1981) Reaction relationships of chrome-spinels in igneous rocks–further evidence from the layered intrusion of Rhum and Mull, Inner Hebrides, Scotland. Contrib Mineral Petrol 78:225–229

Hill B, Roeder P (1974) The crystallization of spinel from basaltic liquid as a function of oxygen fugacity. J Geol 82:709–729

Himmelberg RG, Loney RA (1995) Characteristics and petrogenesis of Alaskan-type ultramafic-mafic intrusions, southeastern Alaska. US Geol Surv Prof Pap 1564:1–47

Himmelberg RG, Loney RA, Craig JT (1986) Petrogenesis of the ultramafic complex at the Blashke Islands, southeastern Alaska. US Geol Surv Bull 1662:1–14

Irvine TN (1965) Chromian spinel as a petrogenetic indicator part 1. Theory. Can J Earth Sci 2:648–672

Irvine TN (1967a) Chromian spinel as a petrogenetic indicator part 2. Petrologic applications. Can J Earth Sci 4:71–103

Irvine TN (1967b) Zoned ultramafic complexes. In: Wylie PJ (ed) Ultramafic and related rocks. John Wiley, New York, pp 83–97

Irvine TN (1973) Bridget Cove volcanics, Juneau Area, Alaska: possible parental magma of Alaskan-type ultramafic complexes. Carnegie Inst Wash Yearb 72:478–491

Ivanov OK (1997) Concentric-zonal pyroxenite-dunite massifs of the Urals (Mineralogy, petrology, genesis). Ekaterinburg, Ural State University 1–488 (in Russian)

Ivanov KS, Shmelev VR (1996) The Platinum Belt of the Urals as a magmatic trace of the early paleozoic subduction zone. Trans Russ Acad Sci/Earth Sci 347A(3):396–399

Iyer K, Austrheim H, John T, Jamtveit JT (2008) Serpentinization of the oceanic lithosphere and some geochemical consequences: constraints from the Leka Ophiolite complex, Norway. Chem Geol 249:66–90

Jackson ED (1969) Chemical variation in coexisting chromite and olivine in chromitite zones of the stillwater complex. In: Wilson HDB (ed) Magmatic ore deposits a symposium, Econ Geol, Monogr 4, pp 41–71

Jan MQ, Khan MA, Windley BF (1992) Exsolution in Al-Cr-Fe^{3+}-rich spinels from the Chilas mafic-ultramafic complex, Pakistan. Am Mineral 77:1074–1079

Kepezhinskas PK, Reuber I, Tanaka H, Miyashita S (1993a) Zoned calc-alkaline plutons in Northeastern Kamchatka, Russia: implications for the crustal growth in magmatic arcs. Mineral Petrol 49:147–174

Kepezhinskas PK, Taylor RN, Tanaka H (1993b) Geochemistry of plutonic spinels from the North Kamchatka Arc: comparisons with spinels from other tectonic settings. Mineral Mag 57:575–589

Kimball KL (1990) Effects of hydrothermal alteration on the composition of chromian spinels. Contrib Mineral Petrol 105:337–346

Krause J (2008) Petrogenetic evolution of Uralian-Alaskan-type mafic-ultramafic complexes in the southern and middle Urals, Russia. PhD-Thesis, University of Mainz, Germany 1–162. http://ubm.opus.hbz-nrw.de/volltexte/2008/1847/

Krause J, Brügmann GE, Pushkarev EV (2007) Accessory and rock forming minerals monitoring the evolution of zoned mafic–ultramafic complexes in the Central Ural Mountains. Lithos 95:19–42

Lattard D, Sauerzapf U, Käsemann M (2005) New calibration data for the Fe-Ti oxide thermo-oxybarometers from experiments in the Fe-Ti-O system at 1 bar, 1000–1300°C and a large range of oxygen fugacities. Contrib Mineral Petrol 149:735–754

Lee YL (1999) Geotectonic significance of detrital chromian spinel: a review. Geosci J 3(1):23–29

Lehmann J (1983) Diffusion between olivine and spinel: application to geothermometry. Earth Planet Sci Lett 64:123–138

Lepage LD (2003) ILMAT: an Excel worksheet for ilmenite-magnetite geothermometry and geobarometry. Comput Geosci 29:673–678

Loferski PJ, Lipin BR (1983) Exsolution in metamorphosed chromite from the Red Lodge district, Montana. Am Mineral 68:777–789

Melcher F, Grum W, Simon G, Thalhammer T, Stumpfl E (1997) Petrogenesis of the ophiolitic giant chromitite deposits of Kempirsai, Kazakhstan: a study of solid and fluid inclusions in chromite. J Petrol 40(10):1419–1458

Mellini M, Rumori C, Viti C (2005) Hydrothermally reset magmatic spinels in retrograde serpentinites: formation of "ferritchromit" rims and chlorite aureoles. Contrib Mineral Petrol 149:266–275

Morse SA (1980) Kiglapait mineralogy II: Fe-Ti oxide minerals and the activities of oxygen and silica. J Petrol 21(4):685–719

Muir JE, Naldrett AJ (1973) A natural occurrence of two-phase chromium-bearing spinels. Can Mineral 11:930–939

Noble JA, Taylor HP (1960) Correlation of the ultramafic complexes of southeastern Alaska with those of North America and the World. 21st International Geological Congress in Copenhagen 1960, Report part 13: 188–197

Ozawa K (1988) Ultramafic tectonite of the Miyamori ophiolitic complex in the Kitakami Mountains, Northeast Japan: hydrous upper mantle in an island arc. Contrib Mineral Petrol 99:159–175

Pang KN, Zhou MF, Lindsley D, Zhao D, Malpas J (2008) Origin of Fe-Ti oxide ores in mafic intrusions: evidence from the Panzhihua intrusion, SW China. J Petrol 49(2):295–313

Pertsev AN, Savelieva GN, Astrakhantsev OV (2000) Magmatic origin of the ultramafic-mafic association of the Kytlym Massif, Platinum Belt of the Urals. Petrol 8(4):370–393

Pinsent RH, Hirst DM (1977) The metamorphism of the Blue River ultramafic body, Cassiar, British Columbia, Canada. J Petrol 18(4):567–594

Power MR, Pirrie D, Andersen JCØ, Wheeler PD (2000) Testing the validity of chrome spinel chemistry as a provenance and petrogenetic indicator. Geology 28(11):1027–1030

Price GD (1980) Exsolution microstructures in titanomagnetites and their magnetic significance. Phys Earth Planet Inter 23:2–12

Pushkarev EV (2000) Petrology of the Uktus dunite-clinopyroxenite-gabbro massif (Middle Urals). Ekaterinburg, Ural Div of RAS

Pushkarev EV, Anikina YV, Garuti G, Zaccarini F, Cabella R (1999) Geikielite (Mg-ilmenite) in association with Cr-spinel and platinoids from the Uktus massif dunite, Middle Urals: genetic implications. Dokl Earth Sci 369A(9):1220–1223

Putnis A (1992) Introduction to mineral sciences. Cambridge University Press, Cambridge

Roeder PL (1994) Chromite: from the fiery rain of chondrules to the Kilauea Iki lava lake. Can Mineral 32:729–746

Roeder PL, Campbell IH (1985) The effect of postcumulus reaction and composition of chrome-spinels from the Jimberlana intrusion. J Petrol 26(3):763–786

Sack RO, Ghiorso MS (1991a) Chromite as a petrogenetic indicator. In: Lindsley DH (ed) Oxide minerals petrogenetic and magnetic significance. Reviews in mineralogy 25 Mineralogical Society of America, Chelsea: pp 323–353

Sack RO, Ghiorso MS (1991b) Chromian spinel as petrogenetic indicators: thermodynamics and petrological applications. Am Mineral 76:827–847

Sack RO, Ghiorso MS (1991c) An internally consistent model for the thermodynamic properties of Fe-Mg-titanomagnetite-aluminate spinels. Contrib Mineral Petrol 106:474–505

Sauerzapf U, Lattard D, Burchard M, Engelmann R (2008) The titanomagnetite-ilmenite equilibrium: new experimental data and thermo-oxybarometric application to the crystallization of basic to intermediate rocks. J Petrol 49(6):1161–1185

Savelieva GN, Pertsev AN, Astrakhantsev OV, Denisova EA, Boudier F, Bosch D, Puchkova AV (1999) Kytlym pluton, north Urals: structure and emplacement history. Geotectonics 33(2):119–142

Savelieva GN, Sharaskin AY, Saveliev AA, Spadea P, Pertsev AN, Babarina II (2002) Ophiolites and zoned mafic-ultramafic massifs of the Urals: A comparative analysis and some tectonic implications. In: Browen D, Juhlin C, Puchkov V (eds) Mountain building in the Uralides: Pangea to the present. Geophys Monogr 132: 135–153

Scowen PAH, Roeder PL, Helz RT (1991) Reequilibration of chromite within Kilauea Iki lava lake, Hawaii. Contrib Mineral Petrol 107:8–20

Speczik S, Wiszniewska J, Diedel R (1988) Minerals, exsolution features and geochemistry of Fe-Ti ores of the Suwalki District (North-East Poland). Miner Depos 23:200–210

Springer RK (1974) Contact metamorphosed ultramafic rocks in the Western Sierra Nevada Foothills, California. J Petrol 15(1):160–195

Tamura A, Arai S (2005) Unmixed spinel in chromitite from the Iwanai-Dake peridotite complex, Hokkaido, Japan: a reaction between peridotite and highly oxidized magma in the mantle wedge. Am Mineral 90:473–480

Tatsumi Y (1989) Migration of fluid phases and genesis of basalt in subduction zones. J Geophys Res 94(B4):4697–4707

Taylor HP, Noble JA (1960) Origin of the ultramafic complexes in southeastern Alaska. 21st International Geological Congress in Copenhagen 1960, Report part 13: 175–187

Taylor HP, Noble JA (1969) Origin of magnetite in the zoned ultramafic complexes of Southeastern Alaska. In: Wilson HDB (ed) Magmatic ore deposits pp 209–230

Thakurta J, Ripley EM, Li C (2008) Geochemical constraints on the origin of sulphide mineralization in the Duke Island Complex, southeastern Alaska. Geochem Geophys Geosystems 9(7)

Turnock AC, Eugster HP (1962) Fe-Al oxides: phase relationships below 1000°C. J Petrol 3(3):533–565

Van der Veen AH, Maaskant P (1995) Chromian spinel mineralogy of the Staré Ransko gabbro-peridotite, Czech Republic, and its implications for sulfide mineralization. Miner Depos 30:397–407